Femtotesla Atomic Magnetometer Employing Diffusion Optical Pumping to Search for Exotic Spin-Dependent Interactions

Wei Xiao, Meng Liu, Teng Wu,* Xiang Peng, and Hong Guo†
State Key Laboratory of Advanced Optical Communication Systems and Networks, School of Electronics, and Center for Quantum Information Technology, Peking University, Beijing 100871, China

(Received 1 September 2022; revised 30 December 2022; accepted 15 February 2023; published 4 April 2023)

Searching for beyond-the-standard-model interactions has been of interest in quantum sensing. Here, we demonstrate a method, both theoretically and experimentally, to search for the spin- and velocity-dependent interaction with an atomic magnetometer at the centimeter scale. By probing the diffused optically polarized atoms, undesirable effects coming along with the optical pumping, such as light shifts and power-broadening effects, are suppressed, which enables a 1.4 $\mathrm{fT_{rms}/Hz^{1/2}}$ noise floor and the reduced systematic errors of the atomic magnetometer. Our method sets the most stringent laboratory experiment constraints on the coupling strength between electrons and nucleons for the force range $\lambda > 0.7$ mm at 1σ confidence. The limit is more than 3 orders of magnitude tighter than the previous constraints for the force range between 1 mm $\sim$ 10 mm, and one order of magnitude tighter for the force range above 10 mm.

DOI: 10.1103/PhysRevLett.130.143201

Introduction.—Exotic spin-dependent interactions that beyond standard model of particle physics have been of interest in the community of quantum sensing in the last decade. These exotic interactions, which may be generated by exchanging hypothetical bosons such as axions [1–3] and axionlike particles [4,5], are introduced to resolve some puzzling questions in fundamental physics, such as the charge-parity (CP) violation in the strong interaction [1,6] and dark matter [7–9]. There are 15 possible exotic spin-dependent interactions between ordinary particles, and they can be divided into two groups: static or velocity-independent interactions, and velocity-dependent interactions [10].

Various approaches have been employed to search for hypothetical spin-dependent interactions, such as torsion balances [11], atomic magnetometers [12–15], nitrogen-vacancy centers in diamond [16,17], magnetic microscopes [18], etc. Recent developments and theoretical motivation in tests of exotic spin-dependent interactions have been reviewed in Refs. [8,19].

In this Letter, we explore a spin- and velocity-dependent interaction for electrons at the centimeter scale with an atomic magnetometer. As one of the most sensitive cryogen-free sensors for measuring magnetic fields, atomic magnetometers can achieve a sensitivity of sub-$\mathrm{fT/Hz^{1/2}}$ [20–22], and they have been adopted to search for various exotic physics, such as spin-gravity interactions [23–25] and dark matter [26]. Nearly all atomic magnetometers working on gas or liquid atoms utilize the optical pumping effect [27,28] to polarize atoms for strengthening the signal amplitude. However, some undesirable effects, such as light shifts [29,30] and power-broadening effects [31], coming along with the optical pumping, are often the dominant sources of systematic errors for atomic magnetometers.

By employing the diffusion optical pumping scheme proposed in this Letter, to overcome these noise and systematic errors, a Rb magnetometer with a sensitivity of 1.4 $\mathrm{fT_{rms}/Hz^{1/2}}$ is realized in the gradiometric mode. Based on the magnetometer, a new constraint on a spin- and velocity-dependent interaction for electrons is established. Herein, we focus on the axial-axial interaction between polarized and unpolarized particles [10], written as

$$V_{4+5} = -f_{4+5}\frac{\hbar^2}{8\pi m_p c}[\hat{\sigma}\cdot(\vec{v}\times\hat{r})]\left(\frac{1}{\lambda r}+\frac{1}{r^2}\right)e^{-r/\lambda}, \qquad (1)$$

where f_{4+5} is a dimensionless coupling strength, $\hbar$ is Planck's constant, m_p is the mass of the polarized electron, c is the speed of light in vacuum, $\hat{\sigma}$ is the spin vector of the polarized electron, $\vec{v}$ is the relative velocity between the polarized and unpolarized particles, $\hat{r} = \vec{r}/r$ is a unit vector of their relative displacement, and λ is the force range. The laboratory upper limits on the coupling strength f_{4+5} are set by works using spin-exchange relaxation-free (SERF) atomic magnetometers [12,15] and slow neutron polarimeters [32].

The axial-axial interaction produces frequency shifts $\Delta\Omega = V_{4+5}/\hbar$ of atomic levels and can also be viewed as an effective magnetic field that can tilt the electron spins, which can be sensitively detected by the atomic magnetometer.

Experiments.—The experimental setup of our scheme to search for exotic spin-dependent interactions is depicted in Fig. 1(a). Since atomic magnetometers with higher sensitivities and fewer systematic errors can set a tighter constraint on the coupling strength f_{4+5}, the atomic

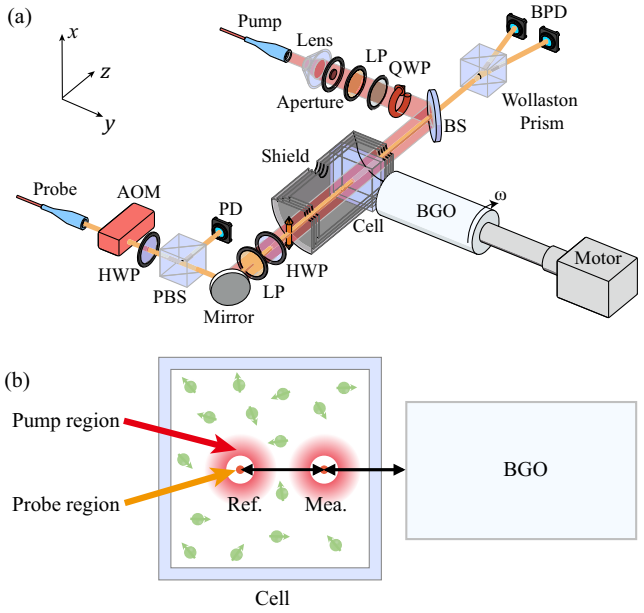

FIG. 1. The experimental setup. (a) The schematic of the atomic magnetometers. A ring-shaped polarized light propagating along the z axis is performed as the pump light to polarize the atoms confined in an atomic vapor cell. For higher sensitivity, the light power is actively stabilized with an acoustic-optical modulator (AOM). An unpolarized BGO crystal is placed next to the Rb vapor cell and rotates around the y axis driven by a stepper motor. BS, beam splitter; LP, linear polarized; QWP, quarter-wave plate; PD, photodiode. For clarity, only one set of the atomic magnetometer is displayed in the figure. (b) The schematic view of the exotic interaction search experiment. The BGO crystal is placed next to the vapor cell at a distance of $L \approx 10$ mm away from the measurement magnetometer. The baseline of the gradiometer is approximately $d \approx 10$ mm.

magnetometer is operated in the SERF regime and further adopts the diffusion optical pumping scheme proposed in this Letter.

For the atomic magnetometer setup, a 795 nm pump light is expanded with a lens to have a diameter of ~6 mm and passes through a 3 mm diameter disc-shaped aperture to make a ring-shaped light. After passing through a linear polarizer and a quarter-wave plate, the ring-shaped light becomes circularly polarized and is employed to optically pump the atoms. The atomic spin polarization is detected with a linearly polarized light based on the optical rotation method [33]. To suppress the intensity noise of the probe light, its power is stabilized with an acousto-optic modulator (AOM). The frequency of the probe light is red detuned about 60 GHz away from the center of the Rb D1 line and the diameter of the probe light is ~1 mm. To separate the pump region and the probe region, the probe light is coaxial to the pump light. In this case, only the atoms in the central region of the ring-shaped pump light that do not directly interact with the pump light can be detected and contribute to the magnetometer signal. The optical rotation of the light after the cell is measured with a balanced photodiode (PD). The ^{87}Rb vapor cell, filled with 600 Torr of N_2 as a buffer gas and a quenching gas, is heated to 153 °C and placed inside a cylindrical magnetic shield. The Helmholtz coils inside the shield generate a parametric modulation field $B_1 \cos \omega t$ along the y axis. The magnetic field can be extracted by demodulating the balanced PD signal with a lock-in amplifier.

Although the atomic spin polarization decays as they diffuse, which leads to a lower polarization in the center region than that in the pump region, such an indirect optical pumping scheme also results in the suppression of power-broadening effects and light shifts. Since the sensitivity of the magnetometer is related to the ratio between the spin polarization and its linewidth, the sensitivity will be improved when the suppression effect of the linewidth broadening is greater than the effect of the decreased polarization. Finally, we find that the polarized atoms in this pumping scheme are more sensitive to the magnetic field, and the sensitivity is increased by a factor of 2–3 compared with the traditional direct optical pumping scheme.

To suppress the thermal magnetic noise generated by the innermost layer of the magnetic shield (μ metal), we need to develop a two-channel magnetometer to suppress the common mode magnetic-field noise from the background. We use the polarizing beam splitter (PBS) to split a beam from the pump (probe) light as the light source of the reference magnetometer (see Supplemental Material [34] for details, which includes Refs. [35,36]). The gradiometer achieves a common-mode rejection ratio (CMRR) of about 30 at 10 Hz. Figure 2(a) shows the performance of the magnetometer, where the magnetic gradiometer achieves a noise floor of 2 $\mathrm{fT_{rms}/Hz^{1/2}}$ with a baseline of 10 mm. Assuming that the remaining noise of the magnetometer is uncorrelated, it implies a sensitivity of 1.4 $\mathrm{fT_{rms}/Hz^{1/2}}$ for each magnetometer. The inset of Fig. 2(a) shows the amplitude-frequency response of the magnetometer, and the −3 dB bandwidth of the magnetometer is measured to be 56 Hz. Furthermore, the magnetometer shows less dependence on the pump light. Figures 2(b) and 2(c) show the dependence of the power-broadening effects and light shifts on the pump light. As a comparison, we further measure the linewidth and the light shift with the aperture that generates the ring-shaped light removed. It can be observed that the undesirable effects from the pump light are largely suppressed when employing the ring-shaped pump light.

With the magnetometer, we conduct a high-sensitivity experiment to search for the exotic frequency shift produced by the exotic interaction V_{4+5}. As shown in Fig. 1(a), the exotic frequency shift is produced by a rotating nonmagnetic $Bi_4Ge_3O_{12}$ (BGO) crystal in our scheme. Because of its high number density (4.3×10^{24} nucleons/cm^3), BGO crystal is frequently taken as an unpolarized nucleon source for searching for exotic spin-dependent interactions

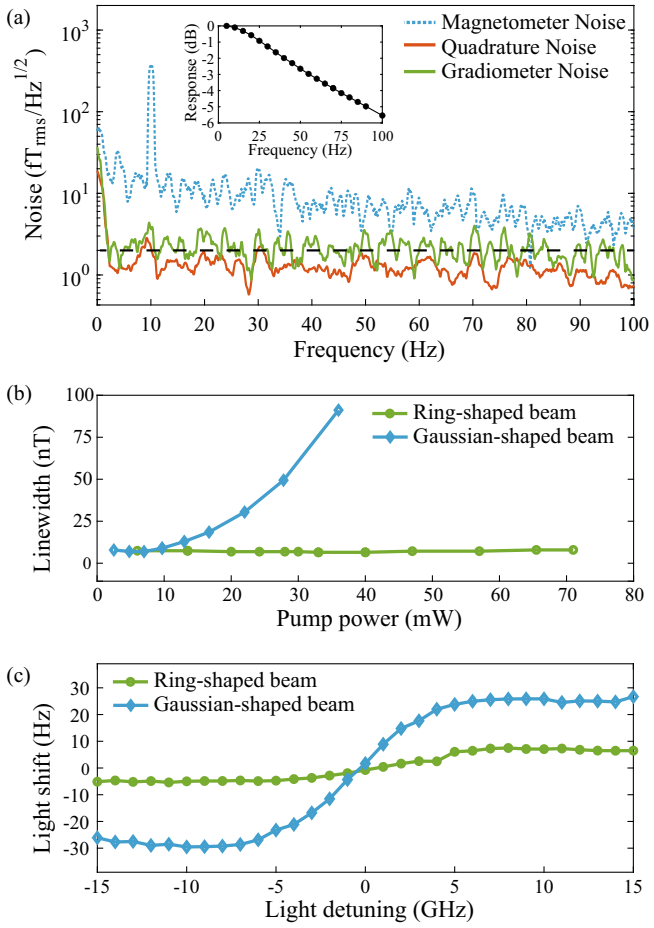

FIG. 2. (a) The typical noise spectral density of the magnetometer. A calibration field with an amplitude of 7 pT at 10 Hz is applied to evaluate the magnetic field sensitivity. Because of the magnetic field noise from the magnetic shield, the magnetometer shows a noise floor of 15 $\mathrm{fT_{rms}/Hz^{1/2}}$ and its quadrature noise shows a low noise floor of 1.4 $\mathrm{fT_{rms}/Hz^{1/2}}$. After suppressing the common-mode magnetic field noise from the surroundings using a gradiometer made up of two individual magnetometers, the magnetic-field sensitivity of the gradiometer reaches 2 $\mathrm{fT_{rms}/Hz^{1/2}}$. The inset shows the amplitude-frequency response of the magnetometer, where the −3 dB bandwidth is about 56 Hz. (b) The dependence of the linewidth of the magnetometer on the pump power. Two cases including the Gaussian-shaped pump beam and the ring-shaped pump beam are included. The linewidth is less sensitive to the pump power in the case of the ring-shaped beam, which indicates the suppression of power-broadening effects. (c) The dependence of the light shift on the pump light detuning. Two cases including the Gaussian-shaped pump beam and the ring-shaped pump beam are included. Weaker light shift effects can be observed in the case of the ring-shaped beam.

[12–14,25,37]. A cylindrical BGO crystal with a length of 60.0 mm and a diameter of 24.0 mm is attached to a graphite rod connected to a stepper motor. The rod rotates around the y axis at a rotation frequency of ν, which is monitored with an optic encoder in real time. As Eq. (1) indicates, only the y-axis effective magnetic field induced by exotic interactions survives in the rotating BGO crystal. To avoid the $1/f$ noise in the magnetometer and obtain a higher signal-to-noise ratio (SNR), the rotation frequency ν is modulated and set to

$$\nu = \nu_0 + \delta\nu \cos \omega t, \tag{2}$$

where ν_0 is the center frequency, $\delta\nu$ is the modulation amplitude, and ω is the modulation frequency. In this case, the exotic frequency shift to be searched for includes an oscillating component. By employing a lock-in detection, where the rotation frequency is taken as the reference signal, the exotic frequency shift $\Delta\Omega$ that is proportional to modulation amplitude $\delta\nu$ can be extracted from the magnetometer signal. The detailed data processing is presented in the Supplemental Material.

As shown in Fig. 1(b), the distance between the center region of the measurement magnetometer and the nearest part of the BGO crystal is set to $L \approx 10$ mm, which is mainly limited by the heat insulation. Recently, several atomic magnetometer-based search experiments for the exotic interaction V_{4+5} [14,37,38] were reported, where the test mass was placed outside the magnetic shield. In this case, the potential noise caused by the rotating BGO crystal can be suppressed by the magnetic shield. However, due to the existence of the magnetic shield, the distance between the vapor cell and the test mass is on the order of tens of centimeters in these experiments, which is more than one order of magnitude larger than the distance in our scheme. As indicated in Eq. (1), a shorter distance enhances the strength of the exotic interaction, especially at smaller force ranges. Although, the gradiometer configuration might be troublesome compared with the single-channel magnetometer, it can suppress the noise and interference caused by the rotating BGO crystal and thus enables a short measuring distance. The baseline between the measurement magnetometer and the reference magnetometer was $d \approx 10.0$ mm. The whole magnetometer apparatus is placed on an optical table that is vibrationally isolated from the mechanical rotation system.

Results.—Figure 3 shows the experimentally measured exotic frequency shift $\Delta\Omega$ obtained with the lock-in algorithm in the case of three different modulation amplitudes $\delta\nu = \{2.40, 2.20, 1.95\}$ Hz. Each data point corresponds to a 2 h measurement and we collected data with different modulation amplitudes for 270 h in total. During data recording, many undesirable noises, such as air vibration, spurious magnetic noise, electronic cross-talk, etc., might contaminate the magnetometer signal. To address this, a fixed enclosure for the rotating BGO crystal is used to reduce the air vibration effect, and a data processing algorithm is designed to suppress the spurious magnetic noise (see Supplemental Material for details).

The insets of Fig. 3 show the histogram of the measured exotic frequency shift $\Delta\Omega$. For example, fitting the histogram in Fig. 3(a) with a Gaussian distribution gives $\Delta\Omega/2\pi = (98 \pm 99)$ nHz. The mean value of the measured exotic frequency shift $\Delta\Omega$ is approximately 1σ from 0,

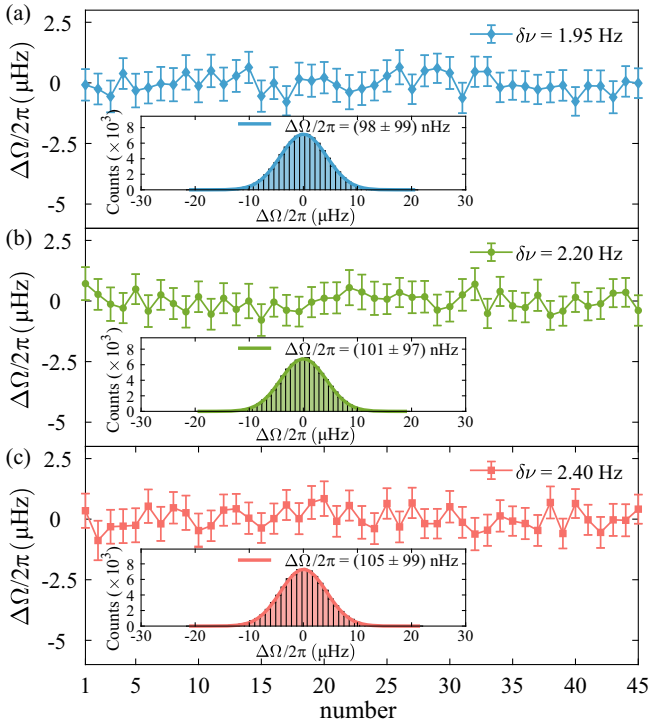

FIG. 3. The measured exotic frequency shift $\Delta\Omega$ for different modulation amplitudes $\delta\nu = 1.95$ Hz (a), $\delta\nu = 2.20$ Hz (b), and $\delta\nu = 2.40$ Hz (c). Each point represents an average over 2 h. These insets show the distribution of the exotic frequency shift $\Delta\Omega$, where the solid line indicates a fit to a Gaussian distribution. The total time duration for recording the data is 270 h.

which indicates that there may be some spurious signal in the measured data. However, by conducting a velocity-dependent experiment, where three different modulation amplitudes are chosen, the velocity-independent spurious signal is largely suppressed (see Supplemental Material for details).

To set a constraint on the coupling strength f_{4+5}, a Monte Carlo integration for the exotic frequency shift is performed based on Eq. (1). The exotic frequency shifts are integrated over the distribution of the unpolarized nucleons in the BGO crystal. The coupling to unpolarized fermions is typically assumed to be the same for neutrons and protons and is 0 for electrons in the unpolarized mass [14,39]. All the measured exotic frequency shifts give a coupling strength of $f_{4+5} = (0.68 \pm 1.08_{\text{stat}}) \times 10^{-23}$ at $\lambda = 0.1$ m. The dominant systematic effects are effectively suppressed to below the statistical sensitivity by eliminating the velocity-independent spurious signal. More details are presented in the Supplemental Material.

The systematic errors of the experiment are summarized in Table I. The major factors leading to errors in our experiments are the instability of the rotation frequency ν and the phase uncertainty between the magnetic field to be measured and the magnetometer outputs. The total systematic error that combines all the uncertainty in these

TABLE I. Estimated contributions of various sources of systematic errors to $\Delta f_{4+5}^{\text{exp}}$.

Parameter	Value	$\Delta f_{4+5}^{\text{exp}}(\times 10^{-23})$[a]
Mass of BGO (g)	201.80 ± 0.02	< 0.001
Amplitude $\delta\nu$ (rad/s)	2.20 ± 0.10	∓ 0.022
Position of BGO L_x (mm)[b]	0.0 ± 1.0	± 0.015
Position of BGO L_y (mm)	10.0 ± 1.0	∓ 0.002
Position of BGO L_z (mm)	0.0 ± 1.0	± 0.015
Baseline d (mm)	10.0 ± 1.0	∓ 0.002
Phase delay (deg)	30.5 ± 5.1	± 0.142
Calibration constant κ (V/nT)	11.20 ± 0.93	∓ 0.042
Final $\Delta f_{4+5}^{\text{exp}}(\times 10^{-23})$	0.68	1.08 (statistical)
($\lambda = 0.1$ m)		0.15 (systematic)

[a]The correction to $\Delta f_{4+5}^{\text{exp}}$ at $\lambda = 0.1$ m.
[b]The origin of coordinates is at the center of the probe light of the measurement magnetometer.

experimental parameters is estimated to be $0.15_{\text{syst}} \times 10^{-23}$, where all of these errors are assumed to be independent [14,40]. Hence, the overall systematic uncertainty can be derived by combining all the systematic errors in quadrature. We quote the final total coupling strength f_{4+5} as $(0.68 \pm 1.08_{\text{stat}} \pm 0.15_{\text{syst}}) \times 10^{-23}$.

Figure 4 shows the experimental constraint on the coupling strength f_{4+5} of the interaction V_{4+5} between unpolarized nucleons and polarized Rb electron spins in the interaction range above 10^{-4} m. The green area represents excluded values at the 1σ level. Our result on the coupling strength with unpolarized nucleons is more than 3 orders of

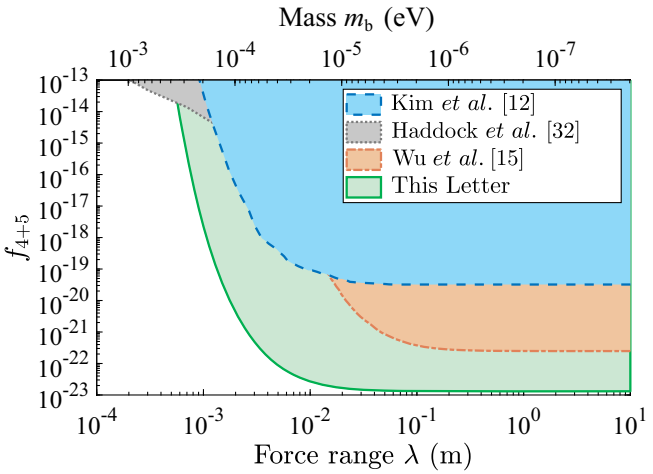

FIG. 4. Experimental constraint (at the 1σ level) on the exotic spin- and velocity-dependent interaction V_{4+5} as a function of the force range λ and mass of the bosons m_b. The blue dashed line is the upper limit established by experiments in Ref. [12]. The orange dash-dotted line is the upper limit established by experiments in Ref. [15]. The gray dotted line is the upper limit established by experiments in Ref. [32]. The green solid line is the upper bound obtained from our experiment, which establishes an improved laboratory bound in the force range from.

magnitude tighter than that of previous works for the range between 1 mm ∼ 10 mm, and one order of magnitude tighter for the range above 10 mm.

Conclusions.—In conclusion, based on the diffusion pumping scheme, we have realized a high-sensitivity Rb magnetometer with a noise floor of 1.4 $fT_{rms}/Hz^{1/2}$. To obtain a better performance of the magnetometer, many efforts have been made to suppress systematic errors. With the diffusion method, our magnetometer is less sensitive to the pump light intensity and frequency detuning compared with the traditional direct optical pumping. To avoid the intensity noise of the probe light, an AOM is employed to actively stabilize the probe light power and we further adopt the optical rotation scheme with a balanced PD to suppress the common-mode noise of the probe light. In addition, because the probe light is far detuned from the center of the Rb D1 line and the absorption line is largely pressure broadened in the buffer-gas-filled vapor cell, the magnetometer is also immune to the probe light frequency noise, as compared with those using an antirelaxation coated vapor cell. The probe light frequency noise could be further suppressed with laser frequency stabilizations. In addition to suppressing the noise inside the magnetometer, a gradiometer configuration is further adopted to suppress the noise from the surroundings, such as the thermal magnetic noise of the magnetic shield, and the magnetic field interference of the rotating BGO crystal. With all of these arrangements, we finally realize a high-sensitivity and stable magnetometer.

The magnetometer is used to search for exotic spin- and velocity-dependent interactions. We have improved the limit on the exotic interaction V_{4+5} between unpolarized nucleons and electrons by several orders of magnitude for the force range above $\sim 10^{-3}$ m.

Because of the advantages of the diffusion optical pumping scheme, which can not only suppress the power-broadening effect and light shifts but also improve the sensitivity of the magnetometer; it can also be helpful in many other applications that are based on atomic vapor cells [41], such as the atomic clock [42,43], the atomic gyroscope [44], and quantum memories [45–47].

This work is supported by the National Natural Science Foundation of China (Grants No. 62071012, No. 61571018, No. 61531003, No. 91436210), the National Science Fund for Distinguished Young Scholars of China (Grant No. 61225003), and National Hi-Tech Research and Development (863) Program. T. W. acknowledges the support from the start-up funding for young researchers of Peking University.

*wuteng@pku.edu.cn
†hongguo@pku.edu.cn

[1] R. D. Peccei and H. R. Quinn, CP Conservation in the Presence of Pseudoparticles, Phys. Rev. Lett. **38**, 1440 (1977).
[2] F. Wilczek, Problem of Strong p and t Invariance in the Presence of Instantons, Phys. Rev. Lett. **40**, 279 (1978).
[3] S. Weinberg, A New Light Boson?, Phys. Rev. Lett. **40**, 223 (1978).
[4] J. Jaeckel and A. Ringwald, The low-energy frontier of particle physics, Annu. Rev. Nucl. Part. Sci. **60**, 405 (2010).
[5] K. Olive, Review of particle physics, Chin. Phys. C **38**, 090001 (2014).
[6] P. Sikivie, Invisible axion search methods, Rev. Mod. Phys. **93**, 015004 (2021).
[7] L. Covi, H. B. Kim, J. E. Kim, and L. Roszkowski, Axinos as dark matter, J. High Energy Phys. 05 (2001) 033.
[8] M. S. Safronova, D. Budker, D. DeMille, D. F. J. Kimball, A. Derevianko, and C. W. Clark, Search for new physics with atoms and molecules, Rev. Mod. Phys. **90**, 025008 (2018).
[9] G. Bertone and D. Hooper, History of dark matter, Rev. Mod. Phys. **90**, 045002 (2018).
[10] B. A. Dobrescu and I. Mocioiu, Spin-dependent macroscopic forces from new particle exchange, J. High Energy Phys. 11 (2006) 005.
[11] J. Ding, J. Wang, X. Zhou, Y. Liu, K. Sun, A. O. Adeyeye, H. Fu, X. Ren, S. Li, P. Luo, Z. Lan, S. Yang, and J. Luo, Constraints on the Velocity and Spin Dependent Exotic Interaction at the Micrometer Range, Phys. Rev. Lett. **124**, 161801 (2020).
[12] Y. J. Kim, P.-H. Chu, and I. Savukov, Experimental Constraint on an Exotic Spin- and Velocity-Dependent Interaction in the Sub-Mev Range of Axion Mass with a Spin-Exchange Relaxation-Free Magnetometer, Phys. Rev. Lett. **121**, 091802 (2018).
[13] Y. J. Kim, P.-H. Chu, I. Savukov, and S. Newman, Experimental limit on an exotic parity-odd spin-and velocity-dependent interaction using an optically polarized vapor, Nat. Commun. **10**, 1 (2019).
[14] H. Su, Y. Wang, M. Jiang, W. Ji, P. Fadeev, D. Hu, X. Peng, and D. Budker, Search for exotic spin-dependent interactions with a spin-based amplifier, Sci. Adv. **7**, eabi9535 (2021).
[15] K. Y. Wu, S. Y. Chen, G. A. Sun, S. M. Peng, M. Peng, and H. Yan, Experimental Limits on Exotic Spin and Velocity Dependent Interactions Using Rotationally Modulated Source Masses and an Atomic-Magnetometer Array, Phys. Rev. Lett. **129**, 051802 (2022).
[16] X. Rong, M. Jiao, J. Geng, B. Zhang, T. Xie, F. Shi, C.-K. Duan, Y.-F. Cai, and J. Du, Constraints on a Spin-Dependent Exotic Interaction Between Electrons with Single Electron Spin Quantum Sensors, Phys. Rev. Lett. **121**, 080402 (2018).
[17] M. Jiao, M. Guo, X. Rong, Y.-F. Cai, and J. Du, Experimental Constraint on an Exotic Parity-Odd Spin- and Velocity-Dependent Interaction with a Single Electron Spin Quantum Sensor, Phys. Rev. Lett. **127**, 010501 (2021).
[18] X. Ren, J. Wang, R. Luo, L. Yin, J. Ding, G. Zeng, and P. Luo, Search for an exotic parity-odd spin- and velocity-dependent interaction using a magnetic force microscope, Phys. Rev. D **104**, 032008 (2021).
[19] F. Ficek and D. Budker, Constraining exotic interactions, Ann. Phys. (Berlin) **531**, 1800273 (2019).

[20] I. Kominis, T. Kornack, J. Allred, and M. V. Romalis, A subfemtotesla multichannel atomic magnetometer, Nature (London) **422**, 596 (2003).
[21] H. Dang, A. C. Maloof, and M. V. Romalis, Ultrahigh sensitivity magnetic field and magnetization measurements with an atomic magnetometer, Appl. Phys. Lett. **97**, 151110 (2010).
[22] D. Sheng, S. Li, N. Dural, and M. V. Romalis, Subfemtotesla Scalar Atomic Magnetometry Using Multipass Cells, Phys. Rev. Lett. **110**, 160802 (2013).
[23] D. F. J. Kimball, I. Lacey, J. Valdez, J. Swiatlowski, C. Rios, R. Peregrina-Ramirez, C. Montcrieffe, J. Kremer, J. Dudley, and C. Sanchez, A dual-isotope rubidium comagnetometer to search for anomalous long-range spin-mass (spin-gravity) couplings of the proton, Ann. Phys. (Berlin) **525**, 514 (2013).
[24] Z. Wang, X. Peng, R. Zhang, H. Luo, J. Li, Z. Xiong, S. Wang, and H. Guo, Single-Species Atomic Comagnetometer Based on ^{87}Rb Atoms, Phys. Rev. Lett. **124**, 193002 (2020).
[25] Y.-K. Feng, D.-H. Ning, S.-B. Zhang, Z.-T. Lu, and D. Sheng, Search for Monopole-Dipole Interactions at the Submillimeter Range with a ^{129}Xe − ^{131}Xe − Rb Comagnetometer, Phys. Rev. Lett. **128**, 231803 (2022).
[26] S. Afach, B. C. Buchler, D. Budker, C. Dailey, A. Derevianko, V. Dumont, N. L. Figueroa, I. Gerhardt, Z. D. Grujić, H. Guo *et al.*, Search for topological defect dark matter using the global network of optical magnetometers for exotic physics searches (gnome), Nat. Phys. **17**, 1396 (2021).
[27] W. Happer, Optical pumping, Rev. Mod. Phys. **44**, 169 (1972).
[28] W. Happer and W. Van Wijngaarden, An optical pumping primer, Hyperfine Interact. **38**, 435 (1987).
[29] B. S. Mathur, H. Tang, and W. Happer, Light shifts in the alkali atoms, Phys. Rev. **171**, 11 (1968).
[30] C. Cohen-Tannoudji and J. Dupont-Roc, Experimental study of zeeman light shifts in weak magnetic fields, Phys. Rev. A **5**, 968 (1972).
[31] M. L. Citron, H. R. Gray, C. W. Gabel, and C. R. Stroud, Experimental study of power broadening in a two-level atom, Phys. Rev. A **16**, 1507 (1977).
[32] C. Haddock *et al.*, A search for possible long range spin dependent interactions of the neutron from exotic vector boson exchange, Phys. Lett. B **783**, 227 (2018).
[33] D. Budker, D. F. Kimball, S. M. Rochester, V. V. Yashchuk, and M. Zolotorev, Sensitive magnetometry based on nonlinear magneto-optical rotation, Phys. Rev. A **62**, 043403 (2000).
[34] See Supplemental Material at http://link.aps.org/supplemental/10.1103/PhysRevLett.130.143201 for details of the experimental setup and the data analysis.
[35] F. Bloch, Nuclear induction, Phys. Rev. **70**, 460 (1946).
[36] S. Appelt, A. B.-A. Baranga, C. J. Erickson, M. V. Romalis, A. R. Young, and W. Happer, Theory of spin-exchange optical pumping of ^{3}He and ^{129}Xe, Phys. Rev. A **58**, 1412 (1998).
[37] K. Y. Wu, S. Y. Chen, J. Gong, M. Peng, and H. Yan, Searching for exotic spin-dependent interactions using rotationally modulated source masses and an atomic magnetometer array, Phys. Rev. D **105**, 055020 (2022).
[38] K. Wei, W. Ji, C. Fu, A. Wickenbrock, J. Fang, V. Flambaum, and D. Budker, New constraints on exotic spin-velocity-dependent interactions, Nat. Commun. **13**, 7387 (2022).
[39] J. Lee, A. Almasi, and M. Romalis, Improved Limits on Spin-Mass Interactions, Phys. Rev. Lett. **120**, 161801 (2018).
[40] A. Almasi, J. Lee, H. Winarto, M. Smiciklas, and M. V. Romalis, New Limits on Anomalous Spin-Spin Interactions, Phys. Rev. Lett. **125**, 201802 (2020).
[41] J. Kitching, S. Knappe, and E. A. Donley, Atomic sensors—a review, IEEE Sens. J. **11**, 1749 (2011).
[42] J. Vanier, Atomic clocks based on coherent population trapping: A review, Appl. Phys. B **81**, 421 (2005).
[43] V. Shah and J. Kitching, Advances in coherent population trapping for atomic clocks, in *Advances in Atomic, Molecular, and Optical Physics*, edited by E. Arimondo, P. Berman, and C. Lin (Academic Press, New York, 2010), pp. 21–74.
[44] T. W. Kornack, R. K. Ghosh, and M. V. Romalis, Nuclear Spin Gyroscope Based on an Atomic Comagnetometer, Phys. Rev. Lett. **95**, 230801 (2005).
[45] D. F. Phillips, A. Fleischhauer, A. Mair, R. L. Walsworth, and M. D. Lukin, Storage of Light in Atomic Vapor, Phys. Rev. Lett. **86**, 783 (2001).
[46] M. Shuker, O. Firstenberg, R. Pugatch, A. Ron, and N. Davidson, Storing Images in Warm Atomic Vapor, Phys. Rev. Lett. **100**, 223601 (2008).
[47] O. Katz and O. Firstenberg, Light storage for one second in room-temperature alkali vapor, Nat. Commun. **9**, 2074 (2018).